Specificity Determinants of a Novel Nck Interaction with the Juxtamembrane Domain of the Epidermal Growth Factor Receptor[†,‡]

Michael J. Hake,[§] Kiattawee Choowongkomon,[||] Olga Kostenko,[||] Cathleen R. Carlin,[||] and Frank D. Sönnichsen*,[||]

Departments of Biochemistry and of Physiology and Biophysics, Case Western Reserve University, Cleveland, Ohio 44106

Received August 2, 2007; Revised Manuscript Received December 20, 2007

ABSTRACT: Nck is a ubiquitously expressed adaptor protein containing Src homology 2 (SH2) and Src homology 3 (SH3) domains. It integrates downstream effector proteins with cell membrane receptors, such as the epidermal growth factor receptor (EGFR). EGFR plays a critical role in cellular proliferation and differentiation. The 45-residue juxtamembrane domain of EGFR (JM), located between the transmembrane and kinase domains, regulates receptor activation and trafficking to the basolateral membrane of polarized epithelia through a proline-rich motif that resembles a consensus SH3 domain binding site. We demonstrate here that the JM region can bind to Nck, showing a notable binding preference for the second SH3 domain. To elucidate the structural determinants for this interaction, we have determined the NMR solution structures of both the first and second Nck SH3 domains (Nck1-1 and Nck1-2). These domains adopt a canonical SH3 β-barrel-like fold, containing five antiparallel strands separated by three loop regions and one 3_{10}-helical turn. Chemical shift perturbation studies have identified the residues that form the binding cleft of Nck1-2, which are primarily located in the RT and n-Src loops. JM binds to Nck1-2 with an affinity of $\sim$80 μM through a positively charged sequence near the N-terminus, as opposed to the polyproline sequence. The two Nck SH3 domains exhibit both steric and electrostatic differences in their RT-Src and n-Src loops, and a model of the Nck1-2 domain complexed with the JM highlights the factors that define the putative binding mode for this ligand.

The epidermal growth factor receptor, the archetypical ErbB[1] receptortyrosine kinase family member, performs a wide range of cellular functions critical for proper growth and development. It plays important roles in the regulation of cell differentiation, proliferation, and epithelial organogenesis (*1*). This receptor must be carefully regulated to maintain a healthy cellular phenotype, as changes in expression patterns have been observed in numerous human cancers (*2*), and developmental defects in several organ systems have been observed in EGFR-deficient transgenic mice (*3, 4*). Many factors contribute to the regulation of EGFR activity, such as the level of protein expression, interactions with other ErbB receptors to form homo- or heterodimers, phosphorylation of selected residues, and internalization leading to lysosomal degradation. Moreover, specific sorting processes help control the distribution of EGFR at the membranes of polarized epithelia. For example, in Madin-Darby canine kidney epithelia, EGF receptors are mainly localized to the basolateral membrane (*5, 6*). Furthermore, EGFR can interact with different adaptor proteins that serve as molecular scaffolds to link the receptor to downstream signaling molecules. A very well-characterized example involves the Grb2 adaptor recruiting the guanine nucleotide exchange factor Sos to autophosphorylated EGFR at the plasma membrane, where Sos can subsequently activate Ras (*7, 8*).

The EGF receptor is an integral transmembrane glycoprotein of 1186 amino acids (*9*). It contains an extracellular N-terminal ligand-binding domain, a single transmembrane helix, a juxtamembrane domain (JM) of approximately 45 residues, a tyrosine kinase domain, and a C-terminal tail. JM contains several intrinsic sorting signals, including basolateral targeting signals such as the ^{667}PLTP^{670} sequence (*10*), and a lysosomal sorting motif (*11*). JM also contains a variety of protein binding sites, including those for calmodulin (*12*), α-subunits of heterotrimeric G_s proteins (*13*), and phosphoinositide kinases (*14*). In addition, JM contains several known phosphorylation sites: these include Thr^{654}, which is a substrate for PKC (*15*), as well as Thr^{669} and Ser^{671}, which are substrates for MAPK (*16, 17*). Furthermore, it was observed that JM can bind to the EGFR substrate and adaptor Eps8 (*18*), which may function in the recruitment of an Eps8-associated signaling protein complex to EGFR. The presence of numerous interaction sites compressed into

[†] This work was supported by National Institutes of Health Grants DK07678 to M.J.H., GM64243 and DK54178 to C.R.C., and GM55362 to F.D.S.

[‡] The coordinates of the first and second human Nck SH3 domains have been deposited in the Protein Data Bank as entries 2JS2 and 2JS0, respectively, and the NMR data have been deposited in the BioMagResBank as entries 15351 and 15349, respectively.

* To whom correspondence should be addressed. Telephone: (216) 368-5405. Fax: (216) 368-1693. E-mail: fds@case.edu.

[§] Department of Biochemistry.

[||] Department of Physiology and Biophysics.

[1] Abbreviations: DCC, deleted in colorectal cancer; EGFR, epidermal growth factor receptor; ErbB, erythroblastic leukemia viral oncogene homologue; GST, glutathione *S*-transferase; HSQC, heteronuclear single-quantum coherence; JM, juxtamembrane domain of EGFR; MALDI-TOF, matrix-assisted laser desorption ionization time-of-flight; MAPK, mitogen-activated protein kinase; NOE, nuclear Overhauser effect; NOESY, nuclear Overhauser effect spectroscopy; PKC, protein kinase C; SH2, Src homology 2; SH3, Src homology 3; 2D, two-dimensional; 3D, three-dimensional.

10.1021/bi701549a CCC: $40.75
Published on Web 02/13/2008

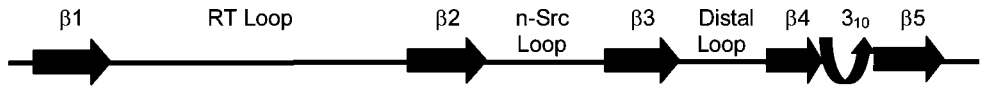

			108	111	121	131	141	151	161	
Nck1-1	4	EVV	VVAK**F**DYVAQ	Q**E**Q**EL**DIKK**N**	ERLWLLDD---S	KS**WW**RVRNSM**N**	KT**G**FV**P**S**NYV**	ERKNS	61
Nck1-2	108	NMP	AYVK**F**NYMAE	R**E**D**EL**SLIK**G**	TKVIVME**K**C--S	DG**WW**RGSYN-**G**	QV**G**WF**P**S**NYV**	TEEGD	165
Nck1-3	192	LHV	VQAL**Y**PFSSS	N**DEEL**NFEK**G**	DVMDVIE**K**PEND	PE**WW**KCRKIN**G**	MV**G**LV**P**K**NYV**	TVMQN	252
Nck2-1	4	EVI	VIAK**W**DYTAQ	Q**D**Q**EL**DIKK**N**	ERLWLLDD---S	KT**WW**RVRNAA**N**	RT**G**YV**P**S**NYV**	ERKNS	61
Nck2-2	113	NIP	AFVK**F**AYVAE	R**E**D**EL**SLVK**G**	SRVTVME**K**C--S	DG**WW**RGSYN-**G**	QI**G**WF**P**S**NYV**	LEEVD	170
Nck2-3	197	LHV	VQTL**Y**PFSSV	T**EEEL**NFEK**G**	ETMEVIE**K**PEND	PE**WW**KCKNAR**G**	QV**G**LV**P**K**NYV**	VVLSD	257
β-PIX	186	QLV	VRAK**F**NFQQT	N**EDEL**SFSK**G**	DVIHVTR**V**E--E	GG**WW**EGTLN-**G**	RT**G**WF**P**S**NYV**	REVKA	243
RacCDC42 GEF6	162	QLI	VKAR**F**NFKQT	N**EDEL**SVCK**G**	DIIYVTR**V**E--E	GG**WW**EGTLN-**G**	RT**G**WF**P**S**NYV**	REIKS	219
Intersectin2	1113	VCQ	VIAM**Y**DYAAN	N**EDEL**SFSK**G**	QLINVMN**K**D--D	PD**WW**QGEIN-**G**	VT**G**LF**P**S**NYV**	KMTTD	1170
Cin85	1	MVE	AIVE**F**DYQAQ	H**DDEL**TISV**G**	EIITNIR**K**E--D	GG**WW**EGQIN-**G**	RR**G**LF**P**D**NFV**	REIKK	58

FIGURE 1: Sequence and secondary structural alignment of the following SH3 domains: three from the Nck1 isoform and three from Nck2, as well as βPIX, RacCDC42 guanine exchange factor 6, Intersectin 2, and Cin85. Boxes encompass the general ligand-binding region on SH3 domains, and bold letters indicate highly conserved positions.

such a small domain stimulates further investigation into their regulation, which can provide key insights into the regulation of the full-length receptor.

Another adaptor protein that plays a role in downstream signaling from EGFR is Nck, which helps regulate numerous intracellular processes, including actin cytoskeletal organization, axonal guidance, DNA synthesis, gene expression, and protein degradation (*19, 20*). Two members of this family, Nck1 and Nck2, are expressed in humans, and a homologue, Dock, occurs in *Drosophila*. These modular proteins each contain three SH3 domains followed by a C-terminal SH2 domain. Nck has been observed to bind the activated, autophosphorylated EGF receptor via its SH2 domain (*21*). Nck simultaneously can utilize its second SH3 module to bind PAK1, a serine/threonine kinase that is a target of Rac1 and Cdc42 (*22–24*), supporting a model of Nck-dependent recruitment of PAK1 to the plasma membrane. Signaling pathways involving PAK kinases, PIX exchange factors, and Nck adaptors lead to Rac1 and Cdc42 activation and actin cytoskeleton regulation, including the formation and disassembly of focal adhesion complexes (*25*). Interestingly, Nck has also been observed to activate Rac1 and regulate axonal guidance in spinal commissural cells via an interaction with the membrane-associated netrin-1 receptor DCC (*26*). This direct interaction was dependent on the SH3 domains, not the SH2 domain, of Nck and occurred in a manner independent of the presence of ligand.

The Nck1 and Nck2 isoforms exhibit a high degree of sequence homology, as they are 68% identical and 79% similar over the entire protein sequence (Figure 1). Despite the high degree of sequence homology, differences in specificity of these two proteins have been observed. For instance, the SH2 domain of Nck2 was demonstrated to bind to phosphorylated ephrin-B, whereas the corresponding domain of Nck1 did not bind (*27*). Distinct preferences for ligand binding have also been observed among the different Nck SH3 domains, contributing to the ability of this adaptor to interact simultaneously with different protein effectors, thus linking membrane receptors to the actin cytoskeleton (*20*). A recent study provided structural insight into the ligand binding preferences of the second and third SH3 domains of Nck2 (*28*), focusing on interacting partners that influence actin cytoskeletal organization and cell movement. In light of the differences observed in the sequences of ligands capable of binding to SH3 domains of Nck2, it is also intriguing to highlight the features that determine the specificity of ligand binding among the SH3 domains of the Nck1 isoform. This study addresses this question while focusing on a novel interaction with JM and discusses the implications of this interaction on downstream signaling pathways.

MATERIALS AND METHODS

Cloning, Expression, and Purification of Proteins. The coding sequences of the Nck1-1 (residues 1–61) and Nck1-2 (residues 107–165) SH3 domains were obtained from a GST−Nck fusion construct. The sequences were amplified by PCR on a Techne Techgene model FTGene5D thermocycler and ligated into the pGEV2 vector (*29*). The following primers were utilized for cloning the Nck1-1 domain: 5′-TCT*GGATCC*ATGGCAGAAGAAGTGGTG-3′ (5′-primer, *Bam*HI restriction site in italics) and 5′-TCC*CTCGAG*TCAACTGTTTTTCCTTTC-3′ (3′-primer, *Xho*I restriction site in italics); the following primers were used for cloning the Nck1-2 domain: 5′-TCT*GGATCC*CTCAACATGCCCGCTTAT-3′ (5′-primer, *Bam*HI restriction site in italics) and 5′-TCC*CTCGAG*TCAGTCACCTTCTTCAGT-3′ (3′-primer, *Xho*I restriction site in italics). The resulting plasmids, pGEV2-Nck1-1 and pGEV2-Nck1-2, each encode a fusion protein consisting of an N-terminal immunoglobulin-binding domain of streptococcal protein G (GB1) linked via a thrombin cleavage site to the Nck SH3 domain of interest. In addition, a pGEV2-Nck1-2 construct bearing the C139S point mutation was generated. Each clone was verified by automated DNA sequencing (Cleveland Genomics, Cleveland, OH). For expression of the unlabeled GB1−Nck1-1 and GB1−Nck1-2 fusion proteins, the plasmids were transformed into competent *Escherichia coli* BL21(DE3) cells. The cells were grown to an OD_{600} of 0.6−0.8, at which point they were induced with 0.3 mM isopropyl β-D-1-thiogalactopyranoside (IPTG) at 37 °C for 4 h. Expression of uniformly ^{13}C- and ^{15}N-labeled GB1−Nck1-1 and GB1−Nck1-2 fusion proteins was achieved by growing the transformed *E. coli* cells in M9 minimal medium supplemented with 1 g/L [^{15}N]ammonium chloride and 2 g/L [^{13}C]glucose as the sole nitrogen and carbon sources, respectively, and the cells were induced as described above. To express biosynthetically directed 10% ^{13}C-labeled Nck domains, M9 minimal medium was prepared as described above but with a combination of 0.2 g/L [^{13}C]glucose and 1.8 g/L unlabeled dextrose as the

sole carbon source. The cells were induced as described above. The cells were harvested by ultracentrifugation and resuspended on ice in a buffer containing 75 mM Tris-HCl, 0.3 M NaCl, 0.2 mM EDTA, and 10 μM butylated hydroxytoluene (pH 7.7). The cells were lysed using standard procedures, including addition of lysozyme and nucleases with sonication. The lysates were centrifuged at 13000 rpm for 30 min. The supernatant was filtered through a 0.22 μM syringe filter, loaded onto an IgG-Sepharose Fast Flow 6 column (GE Healthcare, Piscataway, NJ), and purified according to the manufacturer's instructions. The GB1 moiety was cleaved from the fusion protein by adding biotinylated thrombin (Novagen, San Diego, CA) to a level of 1 unit/mg of fusion protein and then allowing the mixture to incubate at room temperature for 4 h. The Nck SH3 domains were subsequently purified from the GB1 moiety by once more running the mixture on the IgG-Sepharose column, this time collecting the flow-through fractions. Biotinylated thrombin was removed by loading the Nck domain solution onto a HiTrap streptavidin HP column (GE Healthcare) and collecting the flow-through. Finally, samples were dialyzed extensively in water for at least 24 h at 4 °C, whereupon they were flash-frozen and lyophilized. Typical yields of cleaved, double-labeled Nck1-1 or Nck1-2 ranged from 3 to 5 mg/L of culture medium. The protein samples were determined by SDS−PAGE analysis to be at least 90% pure, and the purity was further verified by MALDI-TOF mass spectrometry and by NMR spectroscopy. The Nck1-1 SH3 domain peptide extended from Met^{1} to Ser^{61}, and the Nck1-2 SH3 domain peptide extended from Leu^{107} to Asp^{165}. Both peptides contained an N-terminal extension of Gly-Ser, which resulted from the thrombin cleavage step.

An expression plasmid encoding JM from residue Met^{644} to Ala^{674} was constructed. The primers 5′-TTA*GGATCC*ATGCGAAGGCGC-3′ (5′-primer, *Bam*HI restriction site in italics) and 5′-TAT*CTCGAG*TCAAGCTTCTCCACTGGG-3′ (3′-primer, *Xho*I restriction site in italics), were utilized for PCR amplification as described above, and the insert was subsequently ligated into the pGEV2 expression vector (*29*). The resulting plasmid, pGEV2-JM, encodes the GB1 domain linked via a thrombin cleavage site to JM (Met^{644}−Ala^{674}). This clone was also verified by automated DNA sequencing (Cleveland Genomics). The GB1−JM 644–674 protein was expressed, purified, and cleaved as indicated above, with the only exception being that the thrombin cleavage occurred at 4 °C for 4 h. The JM 644–674 peptide also contained an N-terminal Gly-Ser sequence, resulting from the cleavage with thrombin.

In addition, synthetic JM peptides extending from Arg^{645} to Gly^{672} were prepared by the Molecular Biotechnology Core facility at the Cleveland Clinic Lerner Research Institute (Cleveland, OH). The peptides (JM 645–672) were acetylated at the N-terminus and amidated at the C-terminus, but one of these peptides also comprised an additional N-terminal Cys residue. A further JM 645–672 peptide, which was not acetylated at the N-terminus, was synthesized as described previously (*30*) and used for the in vitro binding assay described below.

NMR Spectroscopy. For Nck1-1 and Nck1-2 domain structure determination, NMR experiments were carried out using Varian INOVA 500 and 600 MHz spectrometers each equipped with a z-shielded triple resonance probe. Protein samples were dissolved in 500 μL of NMR buffer [20 mM NaH_2PO_4 and 100 mM NaCl (pH 6) containing 10% D_2O by volume] to produce a final protein concentration of 0.5−1.0 mM. Because the Nck1-2 domain was observed to form covalent dimers due to oxidation of Cys^{139}, DTT was added to a final concentration of 4 mM, which was sufficient to reduce the protein to monomers, as seen by gel filtration (data not shown). All spectra on Nck domains were recorded at 37 °C. For the assignment of backbone and Cβ resonances, the following NMR experiments were recorded on both domains at 500 MHz: $^{15}N-^{1}H$ HSQC, 3D HNCO, 3D HNCACB, and 3D CBCA(CO)NH (*31*). The assignment of the side chain resonances was achieved with 3D H(C)CH-TOCSY, H(CC)-TOCSY-(CO)NH, and (H)CC-TOCSY-(CO)NH experiments at 37 °C (*32*). NOE restraints for structure calculations were obtained at 600 MHz from ^{15}N-resolved $^{1}H-^{1}H$ NOESY, aliphatic ^{13}C-resolved $^{1}H-^{1}H$ NOESY, and aromatic ^{13}C-resolved $^{1}H-^{1}H$ NOESY experiments, each with a mixing time of 150 ms (*31*). A 2D $^{1}H-^{1}H$ NOESY on a Bruker Avance 600 MHz instrument equipped with a z-shielded gradient triple resonance cryoprobe was performed on both Nck1-1 and Nck1-2 in D_2O to facilitate aromatic side chain assignments. Stereospecific assignments of selected side chain atoms and χ^1 dihedral angle constraints were made using a 3D HNHB experiment for the Nck1-1 domain (*33*). Furthermore, the prochirality of the methyl groups of valine and leucine residues in both domains was determined from samples containing 10% ^{13}C-labeled glucose (*34*). All NMR data were processed using NMRPipe (*35*) and subsequently transferred to NMRView (*36*) for visualization, picking, assignment, and quantification of peaks in the spectra.

Structure Calculations. Ensembles of structures of both the Nck1-1 and Nck1-2 SH3 domains were calculated using CYANA 2.1 (*37, 38*). Inputs for the calculations included unassigned peak lists from the ^{15}N-resolved $^{1}H-^{1}H$ NOESY, and from the aliphatic and aromatic ^{13}C-resolved $^{1}H-^{1}H$ NOESY spectra. In addition, φ and Ψ dihedral restraints for both domains were generated from TALOS (*39*), and HNHB-derived χ^1 constraints were included for Nck1-1. Calibration constants were determined automatically for each peak list. Chemical shift tolerances were set at 0.035 ppm for direct and indirect proton dimensions and at 0.5 ppm for carbon and nitrogen dimensions. A total of 15000 torsion angle dynamics steps were used in calculating each structure. Calculations were performed using the standard protocol of iterative assignment followed by simulated annealing in dihedral angle space, including two and four manually assigned NOEs for Nck1-1 and Nck1-2, respectively. From an ensemble of 100 calculated structures, the 50 structures with the lowest target function from CYANA were then utilized as input for simulated annealing with explicit water refinement using CNS (*40*). Standard parameters and protocols were utilized (*41*). The 20 lowest-energy structures lacking distance violations of >0.3 Å and dihedral violations of $>3°$ were included in the final structural ensemble. Structures were analyzed by PROCHECK-NMR (*42*), and the structures were visualized with either Swiss-PDB Viewer (*43*) or MOLMOL (*44*).

In Vitro Binding Assay. The JM 645–672 peptide with a free N-terminus was coupled to Sepharose beads by using an NHS-activated bead kit (Pierce Chemical Co., Rockford,

IL). GST fusion constructs encoding SH3-containing proteins were obtained from B. Wang (MetroHealth Medical Center, Cleveland, OH). The GST fusion proteins were expressed in *E. coli* and purified using standard protocols. Fusion proteins were eluted from glutathione−agarose beads and dialyzed overnight in a solution of 50 mM Tris (pH 8.0), and the eluted protein was quantified by a Bradford assay. A 5 μg amount of each purified SH3−GST fusion protein was incubated with 0.5 mL of the JM-coupled Sepharose beads in 5% (w/v) evaporated milk and 50 mM Tris buffer (pH 8.0) at 4 °C overnight. The beads were then washed twice with 1 M NaCl and 50 mM sodium carbonate (pH 11.0), and the bound protein was subsequently incubated with SDS sample buffer, boiled, directly analyzed by SDS−PAGE, and visualized by immunoblotting with GST antibodies.

Binding Interactions Analyzed by NMR Titrations. A 100 μM stock solution of the uniformly ^{13}C- and ^{15}N-labeled Nck1-2 SH3 domain was prepared in buffer containing 20 mM NaH_2PO_4 and 100 mM NaCl (pH 6.0). Unlabeled JM 645–672 peptide was added incrementally from a 950 μM stock solution until the JM peptide concentration reached an 8-fold molar excess relative to the Nck1-2 domain. A series of ^{15}N− ^{1}H HSQC spectra was obtained at 37 °C on a Bruker 600 MHz Avance spectrometer equipped with a z-shielded gradient triple resonance cryoprobe, and the chemical shift changes of the Nck1-2 peaks were measured. The total chemical shift change for a given peak was determined from the equation $\delta_{total} = [(\delta_H)^2 + (\delta_N/10)^2]^{1/2}$ (parts per million), where δ_H and δ_N are the chemical shift changes in the proton and nitrogen dimensions, respectively.

The dissociation constant of the interaction of Nck1-2 with JM 645–672 was obtained by plotting the chemical shift changes for seven selected resonances (backbone amides of Arg^{121}, Asp^{123}, Glu^{124}, and Trp^{143} and side chain indoles of Trp^{143}, Trp^{144}, and Trp^{154}) as a function of the molar ratio of ligand to protein. The amount of change at a given data point was expressed as a fraction of the sum of the perturbations over all data points for that peak and then normalized to a 0–100% scale. Curve fitting was accomplished by simultaneous fitting of data from these seven peaks with xcrvfit version 2.1.1 (R. Boyko and B. Sykes, University of Alberta, Edmonton, AB) with the following quadratic equation:

$$[SH3]_{bound} = \left\{K_d + [JM]_{total} + [SH3]_{total} - \left[(K_d + [JM]_{total} + [SH3]_{total})^2 - 4[JM]_{total}[SH3]_{total}\right]^{\frac{1}{2}}\right\}/2 \quad (1)$$

To determine the binding site on JM, a 100 μM solution of uniformly ^{13}C- and ^{15}N-labeled JM 644–674 was prepared in a buffer containing 20 mM NaH_2PO_4 and 100 mM NaCl (pH 5.0). Unlabeled GB1−Nck1-2 fusion protein was added in regular increments from a 500 μM stock solution until the excess unlabeled fusion protein concentration reached an approximately 3-fold molar excess relative to the labeled JM 644–674 peptide. Series of ^{15}N− ^{1}H HSQC and ^{13}C−^{1}H HSQC spectra were obtained at 37 °C, and perturbations of JM peptide peaks were monitored. Chemical shift assignments for the JM peptide were obtained from previously determined values for the JM 645–697 peptide (*45*). The GB1 affinity tag had no discernible effect on the interaction with the JM peptide, which can be deduced from the titration of the JM 645–697 peptide with GB1−Nck1-1 fusion protein (Figure S1 of the Supporting Information). Conversely, addition of JM peptide (JM 645–672) to protein GB1 alone did not lead to discernible chemical shift changes (Figure S2 of the Supporting Information).

Modeling the Nck1-2−JM Complex. The orientation of a PAK2 peptide bound to the βPIX SH3 domain (PDB entry 2DF6) was used as a template to model the interaction of JM with the Nck1-2 domain. First, βPIX (with the PAK2 ligand bound) from residue 11 to 60 and Nck1-2 from residue 111 to 160 were aligned in Swiss PDB Viewer (*43*). The peptide backbone of PAK2 from residue Pro^{180} to Lys^{192} was used as a scaffold to build the JM ligand from Arg^{646} to Leu^{658} by replacing the PAK2 side chains with the corresponding side chains from JM, as done in Swiss PDB Viewer. Subsequently, the ligand backbone conformation was manually optimized in three steps, and brief energy minimizations were performed between and after each manual change (500 steps of steepest descent minimization in GROMOS96 as implemented in SPDBV version 3.7) to remove steric violations in the structural model of the complex. Final visualization of the complex was carried out using MOLMOL (*44*).

To provide independent support for the proposed binding orientation of JM on Nck1-2, an NMR-based titration was performed with a terminally spin-labeled JM peptide, using methods adapted from Mahoney et al. (*46*). Briefly, the JM 645–672 peptide containing an N-terminal cysteine (Cys-JM 645–672) was coupled to the MTSL spin-label in buffer containing 20 mM NaH_2PO_4 and 100 mM NaCl (pH 7.0) at room temperature for 2 h. The resulting MTSL-JM peptide was purified by RP-HPLC, and the presence of the spin-label was verified by EPR spectroscopy and mass spectrometry. For the NMR titrations, the C139S mutant of Nck1-2 was utilized to bypass the inclusion of DTT, which would reduce the MTSL-JM disulfide linkage and thus dissociate the spin-label from the peptide. The Nck1-2 C139S domain binds JM with an affinity similar to that of wild-type Nck1-2 (data not shown). The JM peptide was added to the Nck1-2 C139S domain at a 1:1 molar ratio, and both ^{15}N−^{1}H and ^{13}C−^{1}H HSQC spectra were acquired.

RESULTS

NMR Resonance Assignment of the First and Second SH3 Domains of Nck. The uniformly ^{13}C- and ^{15}N-labeled Nck1-1 and Nck1-2 domains were expressed and purified. The purity of the samples was verified by mass spectrometry and by NMR. The ^{15}N−^{1}H HSQC spectra for the two domains are shown in Figure 2 and are indicative of the excellent data quality obtained for the proteins. Backbone assignments were achieved using an array of triple-resonance experiments as described in Materials and Methods. For the Nck1-1 domain, all resonances were assigned unambiguously, while for Nck1-2, all resonances except for Cys^{139} and Ser^{140} were assigned. These latter residues occur in the n-Src loop, which is a characteristically flexible region of SH3 domains, and are presumed to be exchange broadened. The single proline residue in Nck1-1 and both prolines in Nck1-2 each occur as the trans isomer based on the presence of $H\alpha^{(i)}-H^{\delta\delta'(i+1)}$ NOE cross-peaks and on the difference between C^{β} and C^{γ} chemical shifts (*47*). For the Nck1-1 domain, a second, less

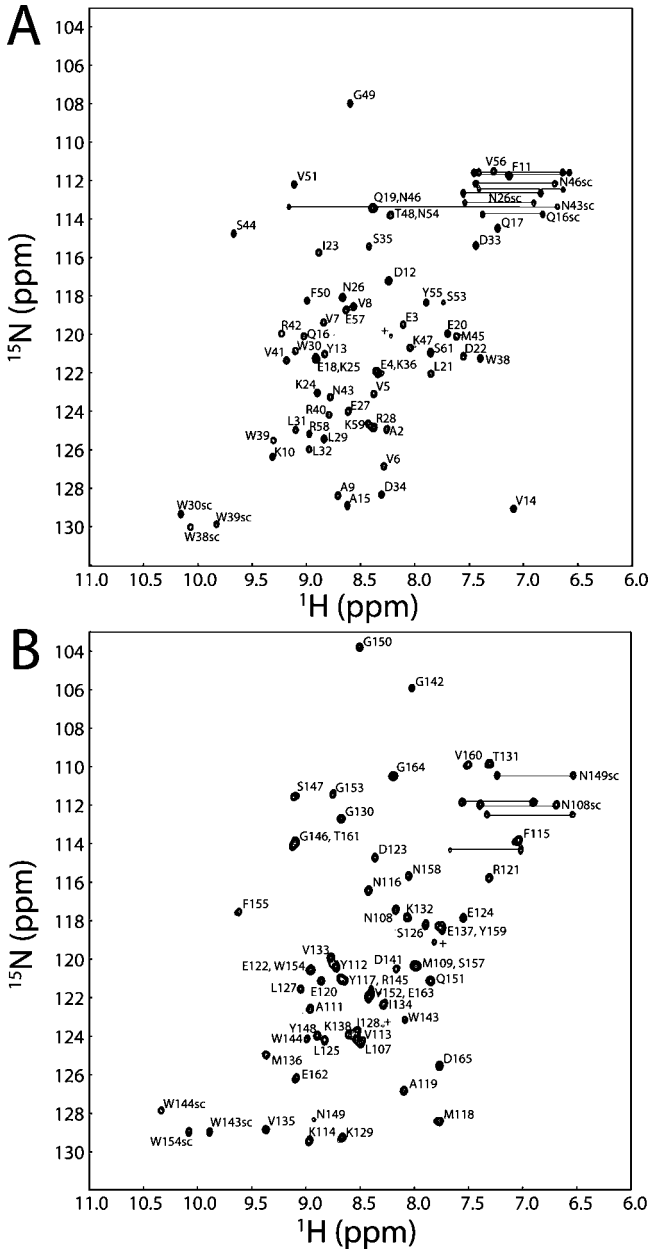

FIGURE 2: ^{15}N−^{1}H HSQC experiments for the Nck1-1 (A) and Nck1-2 (B) SH3 domains showing the backbone assignment for at least 95% of all assignable residues. Side chain peaks are labeled with sc, and peaks labeled with a plus sign originate from a minor, dimeric form of the protein domain.

intense set of peaks was observed at a lower contour level (Figure 2). These peaks were sufficiently weak such that they were not readily observed in the 3D experiments performed on the sample; thus, the presence of these peaks did not interfere with peak picking and analysis for structure calculation. The proportion of protein in the minor form did not exceed a peak intensity ratio of 1:3 between the minor and major forms. According to gel filtration chromatography, the minor form represented a dimeric species while the major form represented a monomer (data not shown). Since the domain lacks cysteine residues, the most likely explanation for dimer formation involves domain swapping, which has been observed in the Eps8 SH3 domain (*48*) and postulated for the homologous first SH3 domain of Nck2 (*49*).

NMR Structure Determination of the First and Second SH3 Domains of Nck. Analysis of chemical shift deviations from random coil values (*50*) for both Nck1-1 and Nck1-2 indicated that the secondary structure of both SH3 domains contains five β-strand regions, consistent with known SH3 structures.

For the Nck1-1 structure calculation with CYANA 2.1, NOE cross-peaks from the 3D ^{13}C- and ^{15}N-resolved NOESY spectra, as well as selected cross-peaks involving aromatic protons from the 2D NOESY spectrum, were included as indicated in Materials and Methods. In addition, 89 dihedral restraints were incorporated: 74 of these were backbone torsion angles obtained from TALOS, and the remaining 15 were χ^1 torsion angles determined from analysis of HNHB cross-peaks. Stereospecific assignments of nine H$^{\beta}$ protons were determined from the HNHB spectrum, and the diastereotopic methyl protons of six of eight valine residues and of all four leucine residues were assigned stereospecifically according to the work of Neri et al. (*34*). After eight iterations of CYANA, 50 structures with the lowest target function were selected for the resulting ensemble, whose target function converged to 0.0039 Å^2 (Table 1), indicating very good agreement between the calculated structures and the experimental data. The 812 assigned NOE distance constraints retained in the CYANA ensemble were distributed relatively evenly across the protein sequence to an average of 13 constraints per residue. This ensemble of 50 Nck1-1 structures was selected for water refinement with CNS. From the water refinement, the 20 lowest-energy structures with no NOE distance violations of >0.3 Å or dihedral angle violations of >3° were selected. Residues Met^1−Val^5 and Lys^{59}−Ser^{61} at the termini were omitted from the final analysis of structure calculations due to their flexibility. The root-mean-square deviation from the mean coordinates from Val^6 to Arg^{58} was 0.40 Å for backbone atoms and 0.96 Å for all heavy atoms (Table 1). Furthermore, 81% of all residues in the ensemble occur in the most favored region of the Ramachandran plot, as indicated by PROCHECK-NMR (*42*).

The same procedure was used for calculating the Nck1-2 SH3 domain structure. For this domain, 66 TALOS-derived φ and Ψ dihedral constraints were incorporated. Stereospecific assignments were included for the H$^{\beta}$ protons of Lys^{138}, Trp^{144}, and Trp^{154}, derived from a manual analysis of intraresidue and sequential H$^{\alpha}$−H$^{\beta}$ and H^{N}−H$^{\beta}$ NOE intensities. Moreover, the diastereotopic methyl protons of all five valine residues and of one of two leucines were assigned stereospecifically as described above (*34*). For Nck1-2, a total of 662 NOE constraints were assigned in the CYANA calculations and the final target function was 0.017 Å^2 (Table 1). Because of the larger proportion of glycine residues in the sequence C-terminal to the n-Src loop, the overall number of NOEs derived from side chain protons in this part of the protein was reduced. Specifically, 14 NOEs per residue were present in the N-terminal half (residues 107–140), while eight NOEs per residue were present in the C-terminal half (residues 141–165). The root-mean-square deviation from the mean coordinates from Met^{109} to Glu^{163} was 0.50 Å for the backbone atoms and 1.01 Å for the heavy atoms (Table 1). In addition, 84% of all residues occur in the most favored region of the Ramachandran plot as determined by PROCHECK-NMR (*42*).

The mean backbone representations of Nck1-1 and Nck1-2, determined from the water-refined ensembles of 20

Table 1: NMR Constraints and Structural Statistics for the Best 20 Structures of Nck1-1 and Nck1-2

	Nck1-1	Nck1-2
total no. of constraints		
NOE constraints		
total	812	662
intraresidue ($i = j$)	222	238
sequential ($\|i - j\| = 1$)	189	125
medium-range ($1 < \|i - j\| < 5$)	68	40
long-range ($\|i - j\| > 5$)	333	259
dihedral angle constraints	89	66
structure statistics from CYANA[a]		
target function (Å^2)	$(3.9 \pm 6.3) \times 10^{-3}$	$(1.7 \pm 2.1) \times 10^{-2}$
structure statistics from CNS[b]		
NOE violations >0.3 Å	0	0
dihedral violations >3°	0	0
total energy (kcal/mol)	−2299 ± 45	−2173 ± 89
NOE constraint energy (kcal/mol)	29 ± 3	27 ± 4
root-mean-square deviation		
from idealized geometry		
bonds (Å)	0.0038 ± 0.0002	0.0035 ± 0.0001
angles (deg)	0.5104 ± 0.0179	0.4659 ± 0.0166
impropers (deg)	1.2321 ± 0.0728	1.2935 ± 0.1586
NOEs (Å)	0.0268 ± 0.0013	0.0284 ± 0.0019
from mean structure[c]		
backbone (N, Cα, C) (Å)	0.40 ± 0.07	0.50 ± 0.08
heavy atoms (Å)	0.96 ± 0.07	1.01 ± 0.10
Ramachandran statistics[d]		
most favored (%)	81.4	84.4
additionally allowed (%)	16.4	13.4
generously allowed (%)	1.4	0.8
disallowed (%)	0.8	1.4

[a] Determined for an ensemble of the 50 structures with the lowest target function. [b] Determined for an ensemble of the 20 lowest-energy structures from refinement in explicit water using standard parameters (*40*). [c] Calculated for residues 6–58 of Nck1-1 and for residues 109–163 of Nck1-2. [d] Taken from PROCHECK-NMR (*41*).

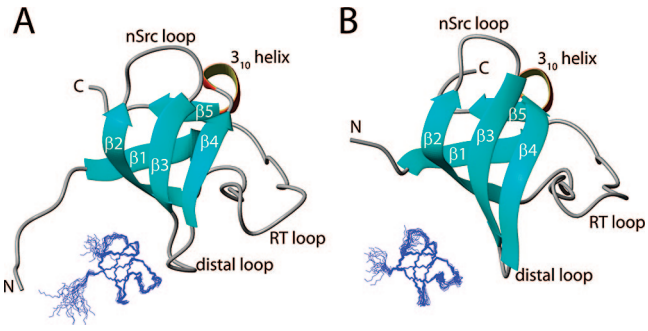

FIGURE 3: Backbone representation of the mean coordinates of both Nck1-1 (A) (PDB entry 2JS2) and Nck1-2 (B) (PDB entry 2JS0). The β-strands, loop regions, and helical segments are indicated for both domains. The β-strands of the Nck1-1 domain occur as follows: β1, Val^6−Ala^9; β2, Arg^{28}−Asp^{33}; β3, Trp^{39}−Arg^{42}; β4, Thr^{48}−Val^{51}; and β5, Val^{56}−Arg^{58}. The β-strands of the Nck1-2 domain occur as follows: β1, Met^{109}−Val^{113}; β2, Lys^{132}−Lys^{138}; β3, Trp^{143}−Tyr^{148}; β4, Gln^{151}−Pro^{156}; and β5, Val^{160}−Glu^{162}. The 3_{10}-helical segments incorporate the following residues: Ser^{53}−Tyr^{55} for Nck1-1 and Ser^{157}−Tyr^{159} for Nck1-2. The water-refined ensembles of the best 20 structures from which the averages were calculated are shown in blue as insets.

structures for each domain, demonstrate the canonical SH3 fold with five β-strands (Figure 3). The β-strands are arranged in each domain as two antiparallel β-sheets arranged at a right angle. One β-sheet consists of strands β1 and β5, along with the first half of strand β2. The other sheet contains the second half of strand β2, followed by strands β3 and β4. A long RT loop separates β1 and β2; a shorter n-Src loop separates β2 and β3, and an even shorter distal loop connects β3 and β4. A single 3_{10}-helical turn that immediately follows the conserved proline residue links strands β4 and β5. The similarity of the backbone architecture of the two domains is reflected in the pairwise rms deviation of 1.8 Å between residues 7−56 of Nck1-1 and 111–160 of Nck1-2. The rms deviation is reduced to 1.0 Å when only the five β-strand regions are included in the comparison.

Identification and Characterization of the EGFR Juxtamembrane Domain as a Nck1-2 Ligand. The EGF receptor serves as the origination point for a significant number of downstream signaling processes influencing cellular growth and differentiation. One such mechanism involves the binding of adaptor proteins to specific regulatory sequences in the receptor. The juxtamembrane domain of EGFR contains a polyproline sequence (^{667}PLTP^{670}), in which the prolines have been shown to be necessary for accurate sorting of the receptor to the basolateral membrane (*10*). This particular sequence resembles a consensus SH3-binding motif, and we therefore examined whether JM was capable of binding an SH3-containing protein. To address this question, an in vitro binding assay was utilized to identify binding partners of a peptide comprising JM. The JM 645–672 peptide was conjugated to Sepharose beads and then incubated with each of several soluble GST fusion proteins, whereupon binding was assessed by Western blotting with an anti-GST antibody. The immunoblots show that the Nck−GST fusion protein, and specifically the Nck1-2 SH3 domain, binds to JM, unlike Src-GST or GST itself (Figure 4). In addition, six other SH3 domains (GrbB2, Crk, Abl, spectrin, p85, and Fgr) were assayed for binding to the JM 645–672 peptide by this method, but no interaction was detected (data not shown).

To specify the region of JM that is responsible for binding to Nck1-2, chemical shift perturbation studies were performed on the ^{15}N- and ^{13}C-labeled JM 644–674 peptide by

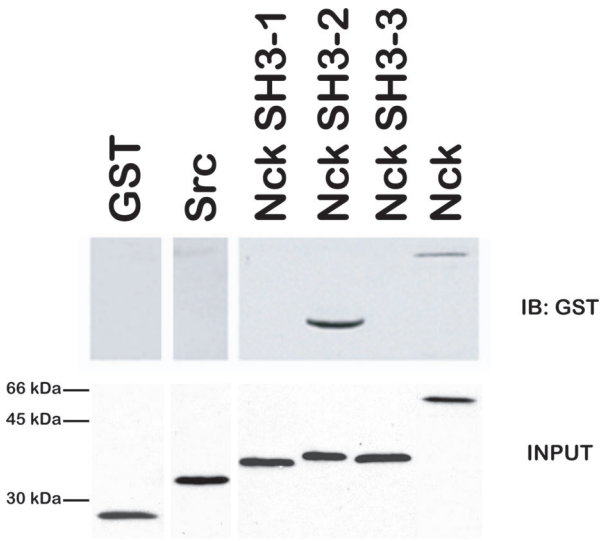

FIGURE 4: In vitro binding assay to identify binding partners of the JM region. The JM 645–672 peptide with a free N-terminal amino group was conjugated to Sepharose beads and incubated with various SH3 domain−GST fusion proteins, as well as with GST alone as a control. The protein complexes were analyzed by SDS−PAGE, and Western blotting with an anti-GST antibody was utilized to detect protein binding. The immunoblots show that Nck (i.e., the Nck1 isoform), and specifically the second SH3 domain, binds to the JM 645–672 peptide. The bottom panel is a loading control showing approximately 5 μg amounts of each purified fusion protein on a Coomassie-stained gel, with molecular masses indicated.

incrementally adding unlabeled GB1−Nck1-2 fusion protein. An overlay of $^{13}C-^{1}H$ HSQC spectra of the JM 644–674 peptide shows prominent broadening of the His^{648} H^{β} and the Ile^{649} methyl proton resonances when Nck1-2 was added to a 3-fold molar excess, in addition to smaller changes for arginine residues (Figure 5A). These residues occur in the N-terminal region of the JM 644–674 peptide. A parallel, $^{15}N-^{1}H$ HSQC-based titration with a longer JM peptide (645–697) (*45*) shows broadening of peaks in the region extending from Arg^{647} to Thr^{654} (Figure 5B), which agrees with the results of a similar titration performed with the JM 644–674 peptide. It is significant that the residues comprising the polyproline sequence (^{667}PLTP^{670}) were not affected by Nck binding. These observations likely indicate that a novel region of JM, in lieu of the proline-rich sequence, is responsible for mediating the interaction. Furthermore, this NMR approach was used to confirm the result from the in vitro binding assay that the second, but not the first, Nck SH3 domain binds to JM (Figure 4). Specifically, the addition of unlabeled Nck1-1 (as a GB1 fusion protein) to a solution of labeled JM 645–697 peptide resulted in no shifting or line broadening of peaks (Figure S1 of the Supporting Information), supporting the observation that the Nck1-1 SH3 domain does not bind JM. This experiment serves as a dual control for the specificity of binding, as it also demonstrates the absence of an interaction between JM and the protein GB1 moiety.

Identification of the JM Binding Site on the Nck1-2 Domain. To identify the binding region on the Nck1-2 domain, chemical shift perturbation experiments were performed with ^{15}N- and ^{13}C-labeled Nck1-2 protein and unlabeled synthetic JM 645–672 peptide. Addition of JM 645−672 to an 8-fold molar excess of Nck1-2 yielded small, yet consistent and saturable, changes for several backbone amide and for all three tryptophan indole resonances (Figure 6A). The binding is consistent with a fast exchange process on the NMR time scale, and this is consistent with the micromolar affinity observed with most SH3 domains and their ligands. Hydrophobic residues encompassing the canonical ligand binding site and charged residues in the specificity pocket between the RT and n-Src loops show the greatest level of perturbation. From the titration data of the backbone amides of Arg^{121}, Asp^{123}, Glu^{124}, and Trp^{143}, as well as the side chain indole peaks of Trp^{143}, Trp^{144}, and Trp^{154}, the amount of chemical shift perturbation was plotted as a function of the molar ratio of the JM 645–672 peptide to the SH3 domain. Fitting these curves (see Materials and Methods) resulted in a binding affinity of 80 $\pm$ 20 μM (Figure 6B). Furthermore, the amount of chemical shift perturbation was determined for all backbone amide resonances at a JM:Nck molar ratio of 2:1 (Figure 6C). These changes were mapped onto the Nck1-2 domain surface according to a color gradient from gray to red with an increasing level of perturbation. The results indicate that the canonical ligand binding site and the specificity pocket located between the RT and n-Src loops exhibit the greatest amount of change (Figure 6D). Residues outside this classical PxxP-binding site of the SH3 domain do not exhibit any significant chemical shift changes, which supports the specificity of this protein–ligand interaction.

Modeling the Nck1-2−JM Complex. The sequence of the Nck1-2 domain is 53% identical and 61% similar to that of the βPIX SH3 domain, on the basis of a BLAST search (*51*). This represents the greatest level of sequence similarity to Nck1-2 among all non-Nck domains whose structure have been determined. The lengths of the RT and n-Src loops of these two domains are identical, and there is 60% sequence identity and 67% similarity among residues comprising the binding cleft (Figure 1). This indicates that the two domains possess largely similar surface topologies. In addition, the pairwise rmsd of Nck1-2 and the βPIX SH3 domain, based on a cocrystal structure of its complex with a PAK2 peptide ligand (*52*), is 1.1 Å among backbone atoms from residue Ala^{111} to Val^{160} of Nck1-2. Therefore, due to its homology to Nck1-2, the βPIX SH3 domain complexed with PAK2 (PDB entry 2DF6) was selected as a template for the Nck1-2−JM interaction. The βPIX surface contains a hydrophobic groove that snugly accommodates the Ile^{183} side chain of the PAK2 peptide. The corresponding residue in JM, Ile^{649}, was selected as the anchor point for overlaying the peptide on the Nck1-2 surface (Figure 7). In addition, charge–charge interactions help to stabilize the βPIX−PAK2 complex, evidenced by the salt bridge that occurs between Arg^{186} of PAK2 and Asp^{23} in the RT loop of βPIX (*52*). Therefore, both hydrophobic and ionic interactions were considered when positioning the JM ligand on the Nck1-2 domain.

In the energy-minimized model of the Nck1-2−JM complex (Figure 7), the aliphatic side chains of Ile^{649} and Val^{650} bind in pockets on the Nck1-2 surface formed by the side chains of Tyr^{117}, Trp^{143}, Pro^{156}, and Tyr^{159}. The side chain of Arg^{651} points away from the Nck1-2 surface in this model, as the backbone atoms of this residue traverse the ridge formed by the Trp^{143} indole ring. The aliphatic portion of the Lys^{652} side chain is stabilized by interactions with the side chain of Trp^{143}, while the ϵ-amino protons fit into a pocket formed by the carboxyl group of Asp^{123}. The

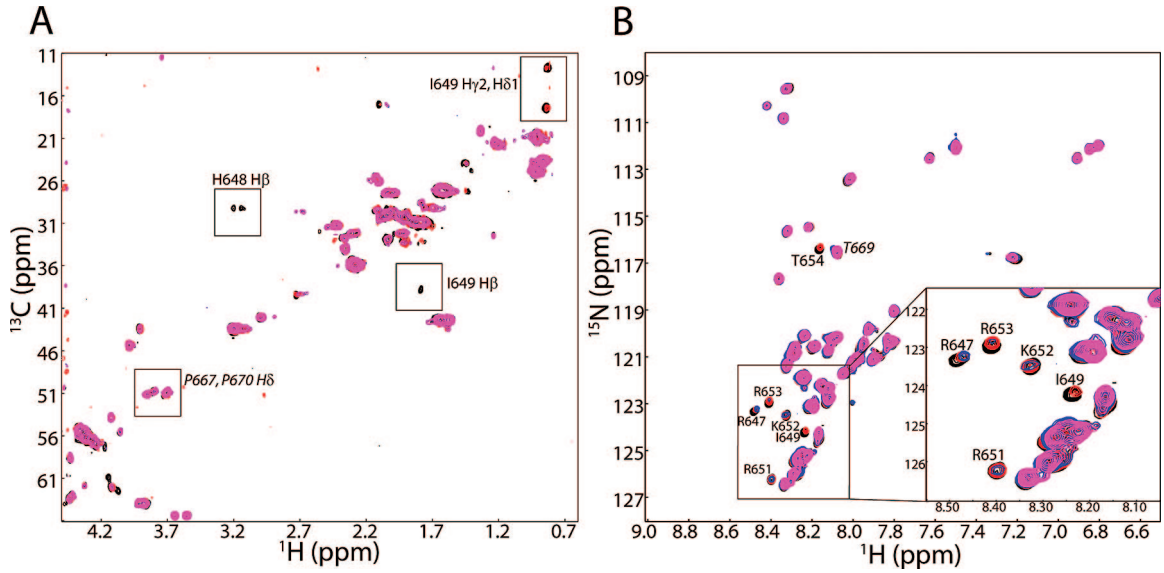

FIGURE 5: (A) Overlay of ^{13}C−^{1}H HSQC spectra showing the ^{13}C- and ^{15}N-labeled JM 644–674 peptide without (black) and with unlabeled GB1−Nck1-2 fusion protein, added in varying amounts up to a 3-fold molar excess (magenta). Peaks showing broadening have bold labels; they were assigned to His^{648} and Ile^{649} protons. The peaks corresponding to the H$^{\delta}$ protons of Pro^{667} and Pro^{670}, which do not change when Nck1-2 is added, are labeled in italics. (B) Overlay of ^{15}N−^{1}H HSQC spectra showing the ^{15}N-labeled JM 645–697 peptide without (black) and with varying amounts of unlabeled GB1−Nck1-2 fusion protein added, up to a 3.2-fold molar excess (magenta). Peaks with bold labels show significant broadening during the titration. The HN peak of Thr^{669}, which does not change when Nck1-2 is added, is labeled in italics. The boxed region of the spectrum is enlarged and shown as an inset.

following residue, Arg^{653}, is positioned so that its side chain can make a favorable charge–charge interaction with the side chain of Asp^{141}. In a manner analogous to the case for the PAK2 ligand, the JM backbone then undergoes a brief helical turn with the side chains of Thr^{654} and Leu^{655} extending into solution. Finally, the two arginine side chains near the C-terminus of the JM ligand, Arg^{656} and Arg^{657}, are both oriented toward the Nck1-2 surface. Specifically, the aliphatic portion of Arg^{656} interacts with the side chains of Trp^{143} and Trp^{154}, and its guanidinium group is positioned close to the carboxyl group of Asp^{141} in the n-Src loop. The Arg^{657} side chain is oriented toward the RT loop, where its guanidinium group is located near the carboxyl group of Asp^{123}.

This binding model was tested empirically via NMR titrations in which a solution of JM peptide containing a site-specific spin-label was added to a solution of isotopically labeled Nck1-2. Because a paramagnetic spin-label causes broadening of resonances of atoms in its proximity, this method provides a direct means of mapping specific peptide ligand residues onto protein binding surfaces (*46*). The JM 645–672 peptide comprising an N-terminal cysteine (Cys-JM 645–672) was coupled via the Cys thiol group to MTSL as described in Materials and Methods. As stated above, the C139S mutant of Nck1-2, which binds JM with similar affinity and in the same region as wild-type Nck1-2, was utilized to bypass the inclusion of DTT in the titrations. The spin-labeled Cys-JM 645–672 peptide was added to the Nck1-2 domain at a 1:1 molar ratio, and overlays of ^{15}N−^{1}H and ^{13}C−^{1}H HSQC spectra show very specific interaction sites (Figure 3 of the Supporting Information). This is evidenced by the fact that only a few of the identified binding cleft residues showed peak broadening, whereas the remaining resonances exhibited only chemical shift perturbations. Resonances assigned to Pro^{156} and Asn^{158} displayed very prominent broadening, and these residues lie toward the left side of the model of the complex (Figure 7). Therefore, since the N-terminal spin-label on the Cys-JM 645–672 peptide occurs in the proximity of these exposed side chain moieties on Nck1-2, the left-to-right orientation of JM in the binding complex model appears reasonable. The reduction of MTSL with 5 mM ascorbic acid caused the reappearance of peaks that had previously been broadened (data not shown), hence confirming that the observed broadening was due to the presence of the spin-label.

DISCUSSION

Protein–protein interactions play a critical role in both intra- and extracellular signaling processes, and adaptor proteins serve to link membrane-associated receptors with downstream intracellular effector molecules. One common interacting module, the SH3 domain, consists of ~60 residues and possesses a conserved folded structure. It is currently estimated that more than 400 such domains are present in the human genome (*53*), thus allowing the integration of numerous cellular signaling networks. The adaptor Nck, which consists of three SH3 domains followed by an SH2 domain, utilizes the specificity of its individual domains to facilitate multiple interactions with different binding partners (*20*). The diversity of Nck binding proteins for a given SH3 domain, as well as the different binding profiles among the three Nck SH3 domains, has motivated recent investigation into the structures of these domains and the determinants that mediate binding specificity. In this study, we determined that the Nck1-1 and Nck1-2 domains adopt the five-stranded β-barrel-like fold typical of SH3 domains (Figure 3). The Nck1-1 structure presented here is very similar to the recently determined NMR structure of the first SH3 domain of Nck2 (PDB entry 2B86) (*49*): the rmsd of the mean backbone coordinates of both ensembles (Val^{6}−Arg^{58} of Nck1-1, Ile^{6}−Arg^{58} of Nck2-1) is 0.9 Å, which is a reasonable value for these homologous domains. As for Nck1-2, the structure

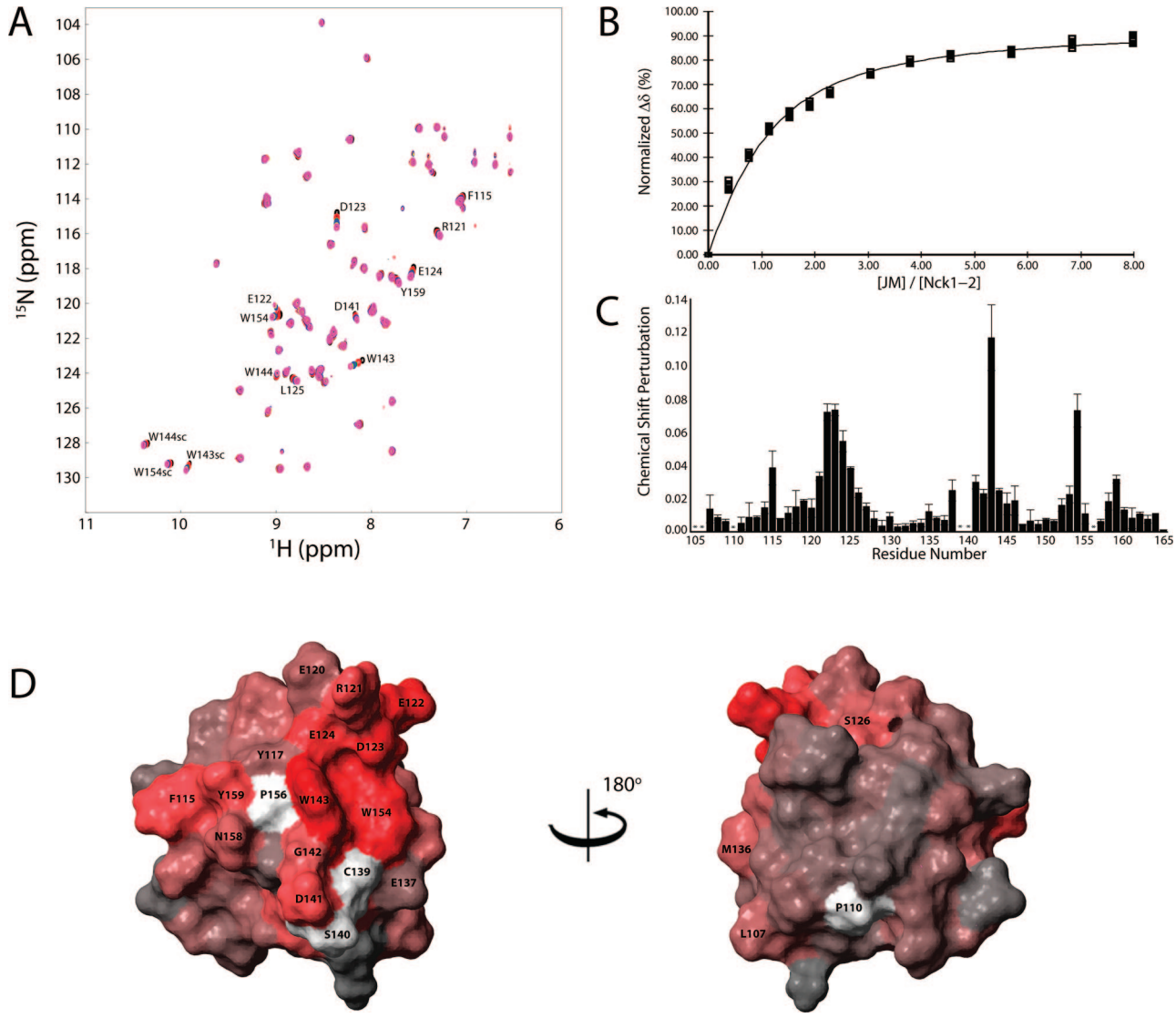

FIGURE 6: (A) Overlay of ^{15}N−^{1}H HSQC spectra of the ^{13}C- and ^{15}N-labeled Nck1-2 domain without (black) and with unlabeled JM 645–672 peptide, added in varying amounts up to an 8-fold molar excess (magenta). Peaks showing chemical shift perturbations are labeled by residue number. (B) Titration curve showing the normalized chemical shift perturbations of seven selected resonances from Nck1-2: the backbone amides of Arg^{121}, Asp^{123}, Glu^{124}, and Trp^{143} and the side chain indole peaks of Trp^{143}, Trp^{144}, and Trp^{154}, plotted as a function of the molar ratio of the JM 645–672 peptide to Nck1-2. (C) Amide chemical shift perturbations of Nck1-2 are indicated for each residue of Nck1-2 upon addition of the JM 645–672 peptide to a 2:1 JM:Nck molar ratio. Perturbations are determined according to the equation $\delta_{total} = [(\delta_H)^2 + (\delta_N/10)^2]^{1/2}$ (parts per million), where δ_H and δ_N are the chemical shift changes in the proton and nitrogen dimensions, respectively. Values are displayed as the average and standard deviation from two separate experiments. Asterisks indicate residues for which no chemical shift information was available. (D) Surface plot of the Nck1-2 domain extrapolating the amount of total backbone amide chemical shift perturbation as a gradient from gray ($\delta_{total} = 0$) to red ($\delta_{total} = 0.12$) onto the surface area of the respective residue. The surface regions colored white are the portions of the surface contributed by Pro^{110}, Cys^{139}, Ser^{140}, and Pro^{156}, for which no amide chemical shift information was available. Pro^{156}, however, experiences chemical shift changes for side chain resonances as seen in ^{1}H−^{13}C HSQC spectra (Figure S3B of the Supporting Information).

presented here is very similar to a recently deposited solution structure in the Protein Data Bank (entry 2CUB), as the similarly determined rmsd of the mean backbone coordinates of these two identical sequences (residues Met^{109}−Glu^{163}) is 0.6 Å.

The specificity of the Nck−JM interaction is exemplified by the observation that, among the SH3 domains tested, only the second SH3 domain of Nck binds to JM (Figure 4). In NMR titrations, the interacting regions of both JM and Nck were localized to a small but well-defined group of residues (Figures 5 and 6). Fitting the Nck chemical shift perturbations to a saturable binding model provides additional evidence for a specific JM−Nck interaction (Figure 6B). The specificity of this interaction also becomes apparent from the negative controls that were performed. For example, the first Nck SH3 domain was observed not to interact at all with JM in NMR titrations using GB1−Nck1-1 fusion protein (Figure S1 of the Supporting Information). By extension, this result confirms that the GB1 affinity tag does not bind the JM peptide. The lack of GB1 binding to JM was also demonstrated in a reciprocal experiment, in which unlabeled JM 645–672 peptide was titrated into a solution of ^{15}N-labeled GB1 (Figure S2 of the Supporting Information). Specificity is further supported by the fact that a JM peptide that extends from residue 677 to 694 and possesses a cluster of positive charges (KKIK) did not bind at all to Nck1-2 (Figure S4 of the Supporting Information). This result

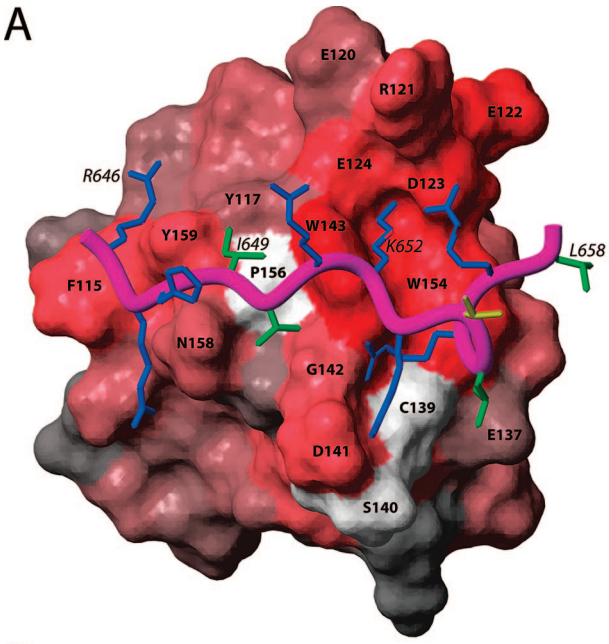

FIGURE 7: (A) Surface plot of the Nck1-2 domain with a model of the bound JM ligand, extending from Arg[646] to Leu[658], across the binding cleft. The coloring of the Nck1-2 domain is the same as in Figure 6, with labels indicated in bold. The model of bound JM is derived from the orientation of the PAK2 peptide ligand in the highly homologous βPIX SH3 domain binding cleft (PDB entry 2DF6). The JM backbone is colored purple; positively charged JM side chains are colored blue and hydrophobic side chains green, and the Thr[654] side chain is colored yellow. Selected JM residues are labeled in italics. (B) Sequence of the PAK2 peptide ligand, as well as the sequence of the JM construct used in our experiments. The isoleucine residue that was used as the anchor point for positioning the ligand on the SH3 domain surface is labeled in bold.

indicates that the presence of a positive charge cluster in a potential ligand for Nck1-2 is not sufficient to enable it to bind.

The difference in binding specificity of JM 645–672 peptide cannot be fully explained by differences in the global fold of each Nck domain, as the pairwise rmsd between Nck1-1 and Nck1-2 (residues 7–56 of Nck1-1, residues 111–160 of Nck1-2) is 1.8 Å. Since the overall SH3 architecture is unchanged, the sequence variations among the three Nck SH3 domains may help to explain these observations. For instance, in pairwise comparisons of the three Nck SH3 domains, sequence identities range between 24 and 29% of all residues, while similarities vary from 53 to 64%. However, the degrees of identity and similarity both increase among the residues comprising the canonical binding region. For example, the level of identity among putative binding cleft residues in the first and second SH3 domains (Nck1-1 and Nck1-2, respectively) is 58%, while their similarity is 79% (Figure 1). Therefore, because the JM binding region on Nck1-2 encompasses the canonical binding cleft (Figure 6B), the specificity must originate from this relatively small proportion of variation in the sequence.

The sequence variability among the Nck SH3 domains is highlighted in the analysis of their surface electrostatic potentials. The electrostatic potentials of the Nck1-1 and Nck1-2 structures determined in this study provide significant insight into the basis of differential ligand binding. The Nck1-2 domain possesses both a neutral region and a highly negatively charged region on its surface (Figure 8B). This surface charge profile resembles that of both the βPIX domain (PDB entry 2DF6) and the Nck2-2 domain (PDB entry 2FRW). The pockets on the surface in the hydrophobic region provide significant complementarity to the Ile[649] and Val[650] side chains of the JM peptide, according to the presented model. The peptide then traverses a small ridge formed from the Trp[143] side chain and interacts via four positively charged side chains (Lys[652], Arg[653], Arg[656], and Arg[657]) with a large negatively charged patch on the Nck1-2 surface. The Nck1-1 domain has a considerably weaker surface negative charge (Figure 8A), as two surface-exposed acidic residues in the RT loop of Nck1-2 (Glu[120] and Asp[123]) are both replaced with glutamine. The Asp[123] side chain carboxyl group is oriented toward two positively charged JM side chains in the presented model (Figure 7). The role of Asp[123] in mediating this interaction is also supported by a large chemical shift perturbation during the NMR titration (Figure 6A). In addition, the Nck1-2 surface region contributed by the side chain of Asp[141] in the n-Src loop is occupied by a lysine (Lys[36]) in Nck1-1, which strongly disfavors an interaction with the positively charged portion of JM proposed to interact in this study. As for the Nck1-3 domain, the structure has not yet been determined. However, the Nck2-3 domain is significantly homologous to Nck1-3, as the two sequences are 73% identical overall and 89% identical among binding cleft residues. Therefore, since the Nck2-3 domain can effectively model the Nck1-3 structure, the electrostatic potential of the structure from Vaynberg et al. was compared to the potentials of the other Nck SH3 domains (Figure 8C) (*54*). Whereas this domain contains an even larger negative patch that could accommodate the arginine and lysine side chains of JM, there are two factors that likely disfavor the interaction. First, the ridge formed by the Trp[229] side chain (analogous to Trp[143] in Nck1-2) protrudes farther from the surface, because the n-Src loop contains two extra residues relative to Nck1-2. This steeper ridge would be predicted to limit the ability of the JM peptide to traverse it and interact with the SH3 domain surface on both sides. Moreover, the large negative patch extends into the region that would be expected to accommodate the hydrophobic side chains of JM, based on the model presented here. Therefore, on the basis of steric constraints and the loss of favorable hydrophobic interactions, binding of JM to Nck2-3 (or Nck1-3) is predicted to occur less favorably than binding to Nck1-2.

The Nck1-2 sequence has been compared to four other sequences of known SH3 domain structures with identical RT and n-Src loop lengths (Figure 1). The rmsd values between Nck and each of these domains, as expected, are relatively small. For instance, the pairwise rmsd for backbone atoms between Nck1-2 and βPIX is 1.1 Å (residues 111–160 of Nck1-2, residues 189–238 of βPIX), again indicating no large-scale regions of deviation from the typical SH3 architecture. As for the primary sequences, βPIX is 53% identical to Nck1-2 over the entire sequence and 60% identical among binding cleft residues, indicating some potential for ligand binding variability. The surface charge profile of βPIX is quite similar to that of Nck1-2; however,

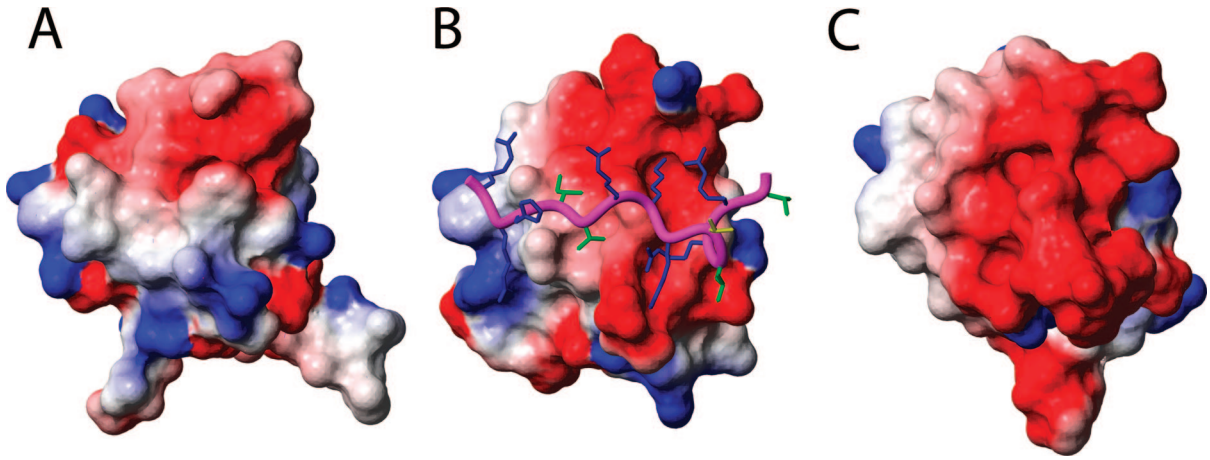

FIGURE 8: Electrostatic surface potentials of the Nck1-1 domain (A) (PDB entry 2JS2) and Nck1-2 domain (B) (PDB entry 2JS0) structures determined here, and the Nck2-3 domain (C) (PDB entry 1U5S) structure. Red represents a negative surface potential, blue a positive surface potential, and white an absence of net surface charge. The JM ligand extending from Arg^{646} to Leu^{658} is positioned on the Nck1-2 domain (B) with the same coloring and orientation as in Figure 7.

there are two residues in the n-Src loop that differ from Nck1-2 with respect to charge. Specifically, the Glu^{137} residue of Nck1-2 is replaced with an arginine in βPIX, and Asp^{141} in Nck1-2 is substituted with a glycine in βPIX. Not only are the loop regions prominent sites of sequence variability (Figure 1), they also possess higher per-residue rms deviations, providing subtle differences in orientation and contributing to the binding of different ligands. Therefore, changes among exposed binding cleft residues, particularly in the RT and n-Src loop regions, may explain why subtle differences in the primary sequence translate into measurable differences in ligand binding affinity among SH3 domains. Toward this end, it will be interesting to determine how well the proposed specificity determinants for the Nck1-2−JM interaction predict the ability of JM to interact with other SH3 domains.

It is significant that the isolated JM binds to Nck1-2 using a sequence outside of the canonical polyproline region. This study represents, to our knowledge, the first example of a non-proline ligand capable of binding to Nck. Several studies have indicated that the PxxP motif is not essential for specific binding to SH3 domains (*55–58*). In the determined cocrystal structure of the C-terminal SH3 domain of Mona/Gads with a peptide ligand from SLP-76, the ligand occupies the canonical PxxP binding site, and its central RxxK motif forms a helical turn (*58*). Even though a 3_{10}-helix is formed in this case, as opposed to a typical polyproline type II helix, this indicates that non-proline peptide ligands traversing the surface of an SH3 domain are capable of forming secondary structure elements to facilitate specific binding. In the case of JM, further investigation is necessary to determine if the JM ligand actually forms a helical turn in the complex, as indicated in our presented model (Figure 7).

The orientation presented for the JM ligand is one possible orientation: because of the symmetry of positive charges on either side of the isoleucine and valine residues that are positioned on the hydrophobic surface patch of Nck1-2, it is possible that the ligand binds in the opposite direction. The model presented in this study was chosen because JM occupies the same orientation as the PAK2 ligand in the complex with βPIX (*52*). Moreover, a greater number of positively charged side chains of JM are able to interact with the negatively charged patch encompassing the RT and n-Src loops, relative to the opposite binding orientation. This model was further corroborated by the pattern of Nck1-2 amide and side chain resonances that were broadened by the addition of a spin-labeled JM peptide. Peaks assigned to Pro^{156} and Asn^{158} showed prominent broadening when an N-terminally MTSL-labeled Cys-JM 645–672 peptide was added to the Nck1-2 domain (Figure S3 of the Supporting Information). This result lends independent support for the left-to-right orientation of JM on the Nck1-2 surface cleft, as these two surface residues are expected to lie in the proximity of the N-terminal portion of JM (Figure 7).

The binding studies described herein were performed with an isolated JM fragment of approximately 30 residues; therefore, the question remains as to whether this interaction occurs in the context of the full-length receptor. The adaptor Nck2 has been observed to interact directly via its SH3 domains with EGFR from A431 epidermoid carcinoma cell lysates, and this interaction occurred in a manner independent of the activation state of the receptor by EGF (*59*). In addition, a constitutive, SH3-mediated interaction of Nck with the netrin-1 receptor DCC was seen in commissural neurons (*26*). In light of these results, it will be interesting to discover if this SH3-mediated interaction of Nck with EGFR JM is also constitutive and if this interaction helps localize Nck near the membrane in unstimulated cells, placing it in position to interact with downstream effectors when the receptor is activated. The midmicromolar Nck−JM binding affinity observed in this study is typical for interactions involving SH3 domains (*60*). This would enable Nck to cycle between JM and other protein ligands, for instance, the PAK1 kinase, contributing to the organization of the actin cytoskeleton and focal complexes (*25, 61*). Many SH3- and SH2-containing adaptors achieve biologically relevant interactions despite relatively low affinities through strategies of combining individual binding events in forming larger protein complexes (*60, 62*). Thus, additional investigation is necessary to elucidate the spatial and temporal regulation of how Nck utilizes all of its modular domains to form large signaling complexes in the cell, while simultaneously taking advantage of the specificity determinants that govern each individual binding event.

ACKNOWLEDGMENT

We thank the Cleveland Center for Structural Biology for the usage of their facilities and Drs. Dale Ray and Xi-An Mao for maintenance of the spectrometers. We also thank Dr. Bingcheng Wang for kindly providing SH3 domain constructs, Drs. Jun Qin and Matthias Buck for critical review of the manuscript, and Dr. Jeffrey Mills for expert technical assistance.

SUPPORTING INFORMATION AVAILABLE

Negative control NMR titration in which the unlabeled GB1−Nck1-1 protein was added to the labeled JM 645–697 peptide (Figure S1), control titration in which unlabeled JM 645–672 peptide was added to labeled protein GB1 (Figure S2), results from titrating an MTSL-labeled JM 645–672 peptide into a labeled Nck1-2 solution (Figure S3A,B), and control titration in which unlabeled JM 677–694 peptide was added to Nck1-2 (Figure S4). This material is available free of charge via the Internet at http://pubs.acs.org.

REFERENCES

1. Carpenter, G. (2000) The EGF receptor: A nexus for trafficking and signaling. *BioEssays 22*, 697–707.
2. Holbro, T., and Hynes, N. E. (2004) ErbB receptors: Directing key signaling networks throughout life. *Annu. Rev. Pharmacol. Toxicol. 44*, 195–217.
3. Threadgill, D. W., Dlugosz, A. A., Hansen, L. A., Tennenbaum, T., Lichti, U., Yee, D., LaMantia, C., Mourton, T., Herrup, K., Harris, R. C., Barnard, J. A., Yuspa, S. H., Coffey, R. J., and Magnuson, T. (1995) Targeted disruption of mouse EGF receptor: Effect of genetic background on mutant phenotype. *Science 269*, 230–234.
4. Sibilia, M., and Wagner, E. F. (1995) Strain-dependent epithelial defects in mice lacking the EGF receptor. *Science 269*, 234–238.
5. Brandli, A. W., Adamson, E. D., and Simons, K. (1991) Transcytosis of epidermal growth factor: The epidermal growth factor receptor mediates uptake but not transcytosis. *J. Biol. Chem. 266*, 8560–8566.
6. Hobert, M., and Carlin, C. (1995) Cytoplasmic juxtamembrane domain of the human EGF receptor is required for basolateral localization in MDCK cells. *J. Cell. Physiol. 162*, 434–446.
7. Buday, L., and Downward, J. (1993) Epidermal growth factor regulates p21ras through the formation of a complex of receptor, Grb2 adapter protein, and Sos nucleotide exchange factor. *Cell 73*, 611–620.
8. Gale, N. W., Kaplan, S., Lowenstein, E. J., Schlessinger, J., and Bar-Sagi, D. (1993) Grb2 mediates the EGF-dependent activation of guanine nucleotide exchange on Ras. *Nature 363*, 88–92.
9. Wells, A. (1999) Molecules in focus: EGF receptor. *Int. J. Biochem. Cell Biol. 31*, 637–643.
10. He, C., Hobert, M., Friend, L., and Carlin, C. (2002) The epidermal growth factor receptor juxtamembrane domain has multiple basolateral plasma membrane localization determinants, including a dominant signal with a polyproline core. *J. Biol. Chem. 277*, 38284–38293.
11. Kil, S. J., and Carlin, C. (2000) EGF receptor residues Leu^{679} Leu^{680} mediate selective sorting of ligand-receptor complexes in early endosomal compartments. *J. Cell. Physiol. 185*, 47–60.
12. Martin-Nieto, J., and Villalobo, A. (1998) The human epidermal growth factor receptor contains a juxtamembrane calmodulin-binding site. *Biochemistry 37*, 227–236.
13. Poppleton, H. M., Sun, H., Mullenix, J. B., Wiepz, G. J., Bertics, P. J., and Patel, T. B. (2000) The juxtamembrane region of the epidermal growth factor receptor is required for phosphorylation of $G\alpha_S$. *Arch. Biochem. Biophys. 383*, 309–317.
14. Cochet, C., Filhol, O., Payrastre, B., Hunter, T., and Gill, G. N. (1991) Interaction between the epidermal growth factor receptor and phosphoinositide kinases. *J. Biol. Chem. 266*, 637–644.
15. Hunter, T., Ling, N., and Cooper, J. A. (1984) Protein kinase C phosphorylation of the EGF receptor at a threonine residue close to the cytoplasmic face of the plasma membrane. *Nature 311*, 480–483.
16. Morrison, P., Takishima, K., and Rosner, M. R. (1993) Role of threonine residues in regulation of the epidermal growth factor receptor by protein kinase C and mitogen-activated protein kinase. *J. Biol. Chem. 268*, 15536–15543.
17. Aifa, S., Johansen, K., Nilsson, U. K., Liedberg, B., Lundstrom, I., and Svensson, S. P. (2002) Interactions between the juxtamembrane domain of the EGFR and calmodulin measured by surface plasmon resonance. *Cell. Signalling 14*, 1005–1013.
18. Castagnino, P., Biesova, Z., Wong, W. T., Fazioli, F., Gill, G. N., and Di Fiore, P. P. (1995) Direct binding of eps8 to the juxtamembrane domain of EGFR is phosphotyrosine- and SH2-independent. *Oncogene 10*, 723–729.
19. McCarty, J. H. (1998) The Nck SH2/SH3 adaptor protein: A regulator of multiple intracellular signal transduction events. *BioEssays 20*, 913–921.
20. Li, W., Fan, J., and Woodley, D. T. (2001) Nck/Dock: An adapter between cell surface receptors and the actin cytoskeleton. *Oncogene 20*, 6403–6417.
21. Li, W., Hu, P., Skolnik, E. Y., Ullrich, A., and Schlessinger, J. (1992) The SH2 and SH3 domain-containing Nck protein is oncogenic and a common target for phosphorylation by different surface receptors. *Mol. Cell. Biol. 12*, 5824–5833.
22. Bokoch, G. M., Wang, Y., Bohl, B. P., Sells, M. A., Quilliam, L. A., and Knaus, U. G. (1996) Interaction of the Nck adapter protein with p21-activated kinase (PAK1). *J. Biol. Chem. 271*, 25746–25749.
23. Galisteo, M. L., Chernoff, J., Su, Y. C., Skolnik, E. Y., and Schlessinger, J. (1996) The adaptor protein Nck links receptor tyrosine kinases with the serine-threonine kinase Pak1. *J. Biol. Chem. 271*, 20997–21000.
24. Lu, W., Katz, S., Gupta, R., and Mayer, B. J. (1997) Activation of Pak by membrane localization mediated by an SH3 domain from the adaptor protein Nck. *Curr. Biol. 7*, 85–94.
25. Buday, L., Wunderlich, L., and Tamas, P. (2002) The Nck family of adapter proteins: Regulators of actin cytoskeleton. *Cell. Signalling 14*, 723–731.
26. Li, X., Meriane, M., Triki, I., Shekarabi, M., Kennedy, T. E., Larose, L., and Lamarche-Vane, N. (2002) The adaptor protein Nck-1 couples the netrin-1 receptor DCC (deleted in colorectal cancer) to the activation of the small GTPase Rac1 through an atypical mechanism. *J. Biol. Chem. 277*, 37788–37797.
27. Cowan, C. A., and Henkemeyer, M. (2001) The SH2/SH3 adaptor Grb4 transduces B-ephrin reverse signals. *Nature 413*, 174–179.
28. Liu, J., Li, M., Ran, X., Fan, J. S., and Song, J. (2006) Structural insight into the binding diversity between the human Nck2 SH3 domains and proline-rich proteins. *Biochemistry 45*, 7171–7184.
29. Huth, J. R., Bewley, C. A., Jackson, B. M., Hinnebusch, A. G., Clore, G. M., and Gronenborn, A. M. (1997) Design of an expression system for detecting folded protein domains and mapping macromolecular interactions by NMR. *Protein Sci. 6*, 2359–2364.
30. Choowongkomon, K., Hobert, M. E., He, C., Carlin, C. R., and Sönnichsen, F. D. (2004) Aqueous and micelle-bound structural characterization of the epidermal growth factor receptor juxtamembrane domain containing basolateral sorting motifs. *J. Biomol. Struct. Dyn. 21*, 813–826.
31. Cavanagh, J., Fairbrother, W. J., Palmer, A. G., III, and Skelton, N. J. (1996) *Protein NMR spectroscopy: Principles and practice*, Academic Press, San Diego.
32. Sattler, M., Schleucher, J., and Griesinger, C. (1999) Heteronuclear multidimensional NMR experiments for the structure determination of proteins in solution employing pulsed field gradients. *Prog. Nucl. Magn. Reson. Spectrosc. 34*, 93–158.
33. Archer, S. J., Ikura, M., Torchia, D. A., and Bax, A. (1991) An alternative 3D NMR technique for correlating backbone nitrogen-15 with side chain Hβ resonances in larger proteins. *J. Magn. Reson. 95*, 636–641.
34. Neri, D., Szyperski, T., Otting, G., Senn, H., and Wuthrich, K. (1989) Stereospecific nuclear magnetic resonance assignments of the methyl groups of valine and leucine in the DNA-binding domain of the 434 repressor by biosynthetically directed fractional ^{13}C labeling. *Biochemistry 28*, 7510–7516.
35. Delaglio, F., Grzesiek, S., Vuister, G. W., Zhu, G., Pfeifer, J., and Bax, A. (1995) NMRPipe: A multidimensional spectral processing system based on UNIX pipes. *J. Biomol. NMR 6*, 277–293.

36. Johnson, B. A., and Blevins, R. A. (1994) NMRView: A computer program for the visualization and analysis of NMR data. *J. Biomol. NMR 4*, 603–614.
37. Güntert, P., Mumenthaler, C., and Wuthrich, K. (1997) Torsion angle dynamics for NMR structure calculation with the new program DYANA. *J. Mol. Biol. 273*, 283–298.
38. Herrmann, T., Güntert, P., and Wüthrich, K. (2002) Protein NMR structure determination with automated NOE assignment using the new software CANDID and the torsion angle dynamics algorithm DYANA. *J. Mol. Biol. 319*, 209–227.
39. Cornilescu, G., Delaglio, F., and Bax, A. (1999) Protein backbone angle restraints from searching a database for chemical shift and sequence homology. *J. Biomol. NMR 13*, 289–302.
40. Brünger, A. T., Adams, P. D., Clore, G. M., DeLano, W. L., Gros, P., Grosse-Kunstleve, R. W., Jiang, J. S., Kuszewski, J., Nilges, M., Pannu, N. S., Read, R. J., Rice, L. M., Simonson, T., and Warren, G. L. (1998) Crystallography & NMR system: A new software suite for macromolecular structure determination. *Acta Crystallogr. D54*, 905–921.
41. Linge, J. P., Williams, M. A., Spronk, C. A., Bonvin, A. M., and Nilges, M. (2003) Refinement of protein structures in explicit solvent. *Proteins 50*, 496–506.
42. Laskowski, R. A., Rullmann, J. A., MacArthur, M. W., Kaptein, R., and Thornton, J. M. (1996) AQUA and PROCHECK-NMR: Programs for checking the quality of protein structures solved by NMR. *J. Biomol. NMR 8*, 477–486.
43. Guex, N., and Peitsch, M. C. (1997) SWISS-MODEL and the Swiss-PdbViewer: An environment for comparative protein modeling. *Electrophoresis 18*, 2714–2723.
44. Koradi, R., Billeter, M., and Wüthrich, K. (1996) MOLMOL: A program for display and analysis of macromolecular structures. *J. Mol. Graphics 14*, 51–55.
45. Choowongkomon, K., Carlin, C. R., and Sönnichsen, F. D. (2005) A structural model for the membrane-bound form of the juxtamembrane domain of the epidermal growth factor receptor. *J. Biol. Chem. 280*, 24043–24052.
46. Mahoney, N. M., Rastogi, V. K., Cahill, S. M., Girvin, M. E., and Almo, S. C. (2000) Binding orientation of proline-rich peptides in solution: Polarity of the profilin-ligand interaction. *J. Am. Chem. Soc. 122*, 7851–7852.
47. Schubert, M., Labudde, D., Oschkinat, H., and Schmieder, P. (2002) A software tool for the prediction of Xaa-Pro peptide bond conformations in proteins based on^{13}C chemical shift statistics. *J. Biomol. NMR 24*, 149–154.
48. Kishan, K. V., Newcomer, M. E., Rhodes, T. H., and Guilliot, S. D. (2001) Effect of pH and salt bridges on structural assembly: Molecular structures of the monomer and intertwined dimer of the Eps8 SH3 domain. *Protein Sci. 10*, 1046–1055.
49. Park, S., Takeuchi, K., and Wagner, G. (2006) Solution structure of the first SRC homology 3 domain of human Nck2. *J. Biomol. NMR 34*, 203–208.
50. Wishart, D. S., and Sykes, B. D. (1994) The^{13}C chemical-shift index: A simple method for the identification of protein secondary structure using^{13}C chemical-shift data. *J. Biomol. NMR 4*, 171–180.
51. Altschul, S. F., Madden, T. L., Schaffer, A. A., Zhang, J., Zhang, Z., Miller, W., and Lipman, D. J. (1997) Gapped BLAST and PSI-BLAST: A new generation of protein database search programs. *Nucleic Acids Res. 25*, 3389–3402.
52. Hoelz, A., Janz, J. M., Lawrie, S. D., Corwin, B., Lee, A., and Sakmar, T. P. (2006) Crystal structure of the SH3 domain of βPIX in complex with a high affinity peptide from PAK2. *J. Mol. Biol. 358*, 509–522.
53. Li, S. S. (2005) Specificity and versatility of SH3 and other proline-recognition domains: Structural basis and implications for cellular signal transduction. *Biochem. J. 390*, 641–653.
54. Vaynberg, J., Fukuda, T., Chen, K., Vinogradova, O., Velyvis, A., Tu, Y., Ng, L., Wu, C., and Qin, J. (2005) Structure of an ultraweak protein-protein complex and its crucial role in regulation of cell morphology and motility. *Mol. Cell 17*, 513–523.
55. Mongiovi, A. M., Romano, P. R., Panni, S., Mendoza, M., Wong, W. T., Musacchio, A., Cesareni, G., and Di Fiore, P. P. (1999) A novel peptide-SH3 interaction. *EMBO J. 18*, 5300–5309.
56. Kang, H., Freund, C., Duke-Cohan, J. S., Musacchio, A., Wagner, G., and Rudd, C. E. (2000) SH3 domain recognition of a proline-independent tyrosine-based RKxxYxxY motif in immune cell adaptor SKAP55. *EMBO J. 19*, 2889–2899.
57. Lewitzky, M., Kardinal, C., Gehring, N. H., Schmidt, E. K., Konkol, B., Eulitz, M., Birchmeier, W., Schaeper, U., and Feller, S. M. (2001) The C-terminal SH3 domain of the adapter protein Grb2 binds with high affinity to sequences in Gab1 and SLP-76 which lack the SH3-typical P-x-x-P core motif. *Oncogene 20*, 1052–1062.
58. Harkiolaki, M., Lewitzky, M., Gilbert, R. J., Jones, E. Y., Bourette, R. P., Mouchiroud, G., Sondermann, H., Moarefi, I., and Feller, S. M. (2003) Structural basis for SH3 domain-mediated high-affinity binding between Mona/Gads and SLP-76. *EMBO J. 22*, 2571–2582.
59. Tu, Y., Li, F., and Wu, C. (1998) Nck-2, a novel Src homology2/3-containing adaptor protein that interacts with the LIM-only protein PINCH and components of growth factor receptor kinase-signaling pathways. *Mol. Biol. Cell 9*, 3367–3382.
60. Mayer, B. J. (2001) SH3 domains: Complexity in moderation. *J. Cell Sci. 114*, 1253–1263.
61. Bagrodia, S., and Cerione, R. A. (1999) Pak to the future. *Trends Cell Biol. 9*, 350–355.
62. Ladbury, J. E., and Arold, S. (2000) Searching for specificity in SH domains. *Chem. Biol. 7*, R3–R8.

BI701549A